# Voltage-Dependent Formation of Anion Channels by Synthetic Rigid-Rod Push – Pull $\beta$-Barrels

**Naomi Sakai,* David Houdebert, and Stefan Matile*[a]**

**Abstract:** Ion channels formed by *p*-octiphenyls equipped with amphiphilic, cationic tripeptide strands and either with (**5**) or without (**6**) axial dipole moment are described (preliminary communication: N. Sakai, S. Matile, *J. Am. Chem. Soc.* **2002**, *124*, 1184 – 1185). Fluorescence kinetics with variably polarized neutral or anionic vesicles, together with planar bilayer conductance measurements, reveal voltage dependence with weakly lyotropic anion selectivity, and deactivation by competing surface potentials of the ion channels formed by asymmetric **5**. In planar bilayers, **5** forms short-lived, poorly organized channels—similar to those produced by $\alpha$-helical natural antibiotics—capable of transforming into stable, ohmic *p*-octiphenyl "$\beta$-barrel" ion channels similar to those of the $>99\,\%$ homologous but symmetric **6**. Fluorescence depth quenching and circular dichroism studies confirm the effect of membrane potentials in promotion of the partitioning of **5** (but not **6**) into the bilayers, identifying partitioning as the voltage-dependent step.

**Keywords:** antibiotics · ion channels · membrane potential · molecular recognition · supramolecular chemistry

## Introduction

Resistance of pathogenic bacteria to common antibiotics has intensified scientific interest in natural antibiotics.[1] As these compounds have not caused resistance despite their long existence, understanding of their mode of action might be expected to result in the development of new, resistance-free antibiotics. It is widely believed that these usually cationic peptides act by selective ion channel formation in the anionic and highly polarized bacterial plasma membranes. Interest in this mechanism of action has, in part, stimulated recent efforts to expand the structural diversity of voltage-dependent ion channels from $\alpha$-helical[2] and $\beta$-helical peptide models[3] to systems with non-peptidic scaffolds.[4, 5] In synthetic ion channels **1** and **2**, the axial macrodipole believed to account for voltage gating is introduced by asymmetric distribution of terminal negative charges (Figure 1).[5] The observed macroscopic voltage dependence (**1**)[5a] and the single-channel current rectification (**2**)[5b] were explained in terms of pores formed by parallel self-assembly directed by dominant dipole – potential interactions.

In the uncharged *p*-octiphenyls **3** and **4**, axial asymmetry is introduced by the presence of $\pi$ donors X and $\pi$ acceptors Y at each end of the rigid-rod scaffold.[6] Push – pull rods **3** and **4** can function as monomers because the lateral azacrowns act as unimolecular ion-conducting relays. This characteristic facilitated the direct correlation of activity and structure in the bilayer. Although examination of the voltage dependence

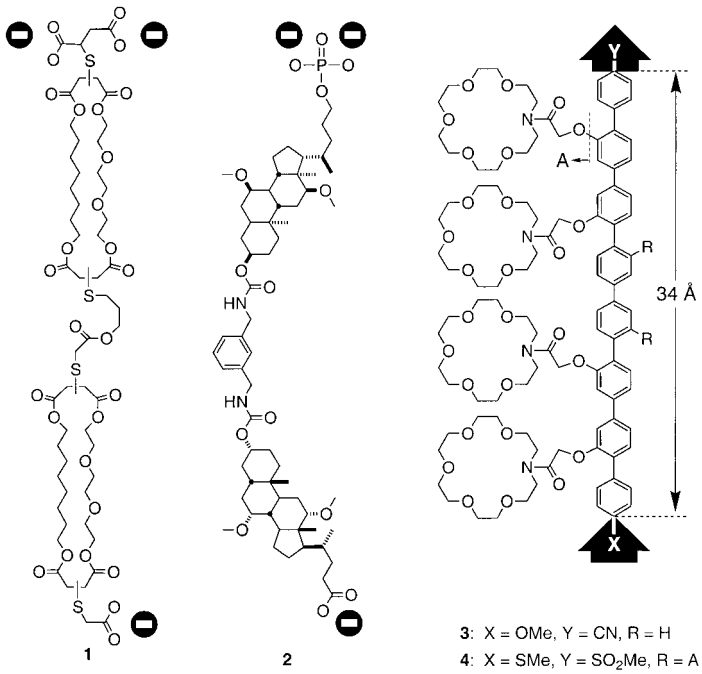


Figure 1. Voltage-dependent synthetic ion channels constructed from flexible (**1**) and semi-rigid (**2**) anionic bolaamphiphiles and neutral rigid push – pull rods (**3** and **4**).

[a] Dr. N. Sakai, Prof. Dr. S. Matile, D. Houdebert
Department of Organic Chemistry, University of Geneva
1211 Geneva 4 (Switzerland)
Fax: (+41) 22-328-7396
E-mail: naomi.sakai@chiorg.unige.ch, stefan.matile@chiorg.unige.ch

 © 2003 WILEY-VCH Verlag GmbH & Co. KGaA, Weinheim 0947-6539/03/0901-0223 $ 20.00+.50/0 

of these push–pull rods on the structural level provided valuable insights into the molecular mechanisms of voltage-gating, the relatively low activity and selectivity led us to examine other pore-forming motifs. It was envisioned that voltage-directed parallel self-assembly of rigid push–pull rods **5** into push–pull $\beta$-barrels $\mathbf{5}^{\uparrow\uparrow\uparrow\uparrow}$ might result in voltage-dependent ion channels with the high activity of symmetric rigid-rod $\beta$-barrels[7] and supramolecular amplification of the selectivity of push–pull *p*-octiphenyls (Figure 2).

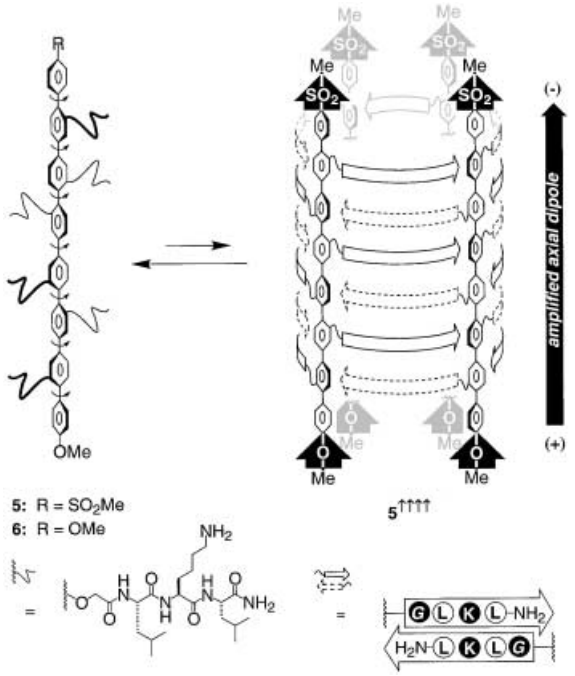


Figure 2. Structures of rigid push–pull rod **5** and push–push rod **6**, and putative suprastructure of parallel $\beta$-barrel $\mathbf{5}^{\uparrow\uparrow\uparrow\uparrow}$. Possible atropisomerism in **5**/**6** is indicated with curved arrows, $\beta$-sheets in $\mathbf{5}^{\uparrow\uparrow\uparrow\uparrow}$ are given as arrows pointing to the C-terminus, amino acid residues (one-letter abbreviation, $G = -OCH_2CO-$) pointing toward the barrel exterior are black on white, internal residues white on black.

Initial studies in SUVs composed of EYPC with inside-negative membrane potentials revealed non-linear voltage and concentration dependence for the formation of tetrameric pores by asymmetric rod **5**. Replacement of the methylsulfone π acceptor in **5** by the methoxy π donor in symmetric rod **6** with nearly identical global structure annihilated the voltage dependence (Figure 2).[8] Here we report comparative studies on the activity of push–pull rod **5** in spherical (SUVs) and planar EYPC bilayers (BLMs) with the use of the symmetric homologue **6**, melittin,[1b, 9] and gramicidin A[3] as control channels. Consistent results from both systems reveal voltage-dependent formation of anion channels by push–pull rod **5** in neutral EYPC bilayers. Inconsistency between the maximal hysteresis found in macroscopic *I*/*V* curves and short-lived single-channel currents in BLMs indicates that voltage-dependent formation of stable push–pull $\beta$-barrels $\mathbf{5}^{\uparrow\uparrow\uparrow\uparrow}$ occurs through a short-lived suprastructure similar to the ion channels formed by $\alpha$-helical peptides. FDQ and CD performed under comparable conditions with polarized SUVs consistently show favored partitioning of **5** into bilayers with inside-negative membrane potentials. These spectroscopic data support the voltage gating mechanism proposed for alamethicin,[10] in which the voltage-dependent step is partitioning of the channel-forming molecule into the bilayer.

## Results

**Activity of rigid push–pull $\beta$-barrels in polarized spherical EYPC/EYPG bilayers**: The activity and selectivity of push–pull rod **5** in spherical bilayers were studied by using uniformly sized (ca. 68 nm) EYPC/EYPG-SUVs containing an internal, pH-sensitive HPTS label and an external, potential-sensitive safranin O label (Figure 3).[11] The desired potassium diffusion potentials were applied by adjustment of the extravesicular concentration of KCl and subsequent addition of $K^+$-carrier valinomycin. These Nernst potentials were verified by the increase in the emission intensity of safranin O (Figure 4c and d, bottom traces) and quantified with calibration curves.[8, 12] Subsequent application of a pH gradient completed the setup for monitoring the decay of pH gradient and membrane potential simultaneously.

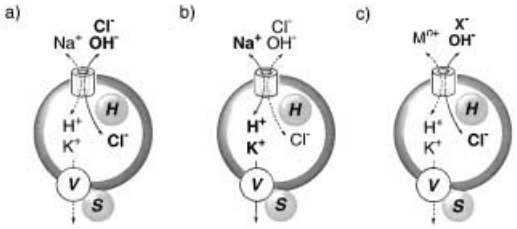


Figure 3. Schematic representation of the assay used to study push–pull rod **5** and controls in polarized EYPC/EYPG-SUVs. Solid arrows/bold ions: favorable antiport with anion- (a, c) and cation-selective (b) pores (dotted arrows: unfavorable antiport, *H* = internal HPTS, *S* = external safranin O, *V* = valinomycin; ions at low concentration are omitted for clarity).

The collapse of pH and $K^+$ concentration gradient (i.e., membrane potential) was monitored by triple-channel fluorescence kinetics to determine ratiometric changes in emission intensity of HPTS in two channels (Figure 4c and d, top traces, one channel not shown) and those of safranin O in the third channel (Figure 4c and d, bottom traces). By comparing activities at various Nernst potentials, it was possible to derive macroscopic activity-potential relationships (Figure 4a and b).

The results with **5** and **6** (Figure 4a and b, solid) have been reported previously.[8] In brief, the capacity of **5** (but not **6**) to transport $H^+/OH^-$ ions across the bilayer was highly voltage-dependent, with *e*-fold increase every −30.4 mV (Figure 4a, solid). The safranin channel, however, showed an almost unchanged membrane potential during the collapse of pH gradient mediated by **5** (or **6**).[8] This result indicated that transport of $H^+/OH^-$ is faster than that of $K^+$, or in other words, anion-selective $OH^-/Cl^-$ antiport through pore **5** (and **6**, Figure 3a). The fourth-power dependence on monomer concentration $c_M$ at $V = -180$ mV suggested that tetrameric aggregate $\mathbf{5}^{\uparrow\uparrow\uparrow\uparrow}$ is the active structure (Figure 2).[8]

Here we report that the characteristics of melittin in triple-channel fluorescence kinetics are quite similar to those


© 2003 WILEY-VCH Verlag GmbH & Co. KGaA, Weinheim
0947-6539/03/0901-0224 $ 20.00+.50/0 *Chem. Eur. J.* **2003**, *9*, No. 1

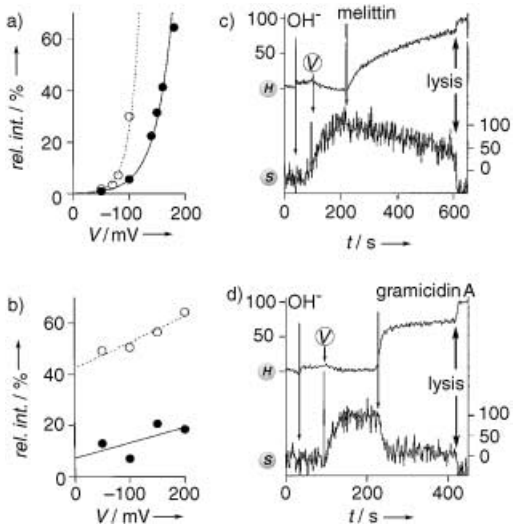


Figure 4. a) and b) Dependence of activity of *p*-octiphenyl **5** (a, ●), melittin (a, ○), *p*-octiphenyl **6** (b, ●), and gramicidin A (b, ○) on membrane potential *V* with exponential (a) and linear (b) curve fits; data for **5** and **6** are from ref. [8]. c) and d) Representative original traces for data in a/b, showing changes in emission intensity of EYPC-SUV entrapped HPTS (top, $\lambda_{exc}=450$ nm, $\lambda_{em}$ 510 nm) and extravesicular safranin O (bottom, $\lambda_{exc}=522$ nm, $\lambda_{em}=581$ nm) as a function of time during addition of safranin O (6 nM), NaOH (5 mM), valinomycin (*V*, 0.6 μM), sample [c: melittin (20 nM), d: gramicidin A (0.2 μM)] and excess melittin (lysis, 1 μM). For original traces of **5**, see Supporting Information of ref. [8].

reported previously for push–pull supramolecule **5**[↑↑↑↑]. Namely, voltage-dependent collapse of the pH gradient occurred before membrane depolarization (Figure 4c). Flux experiments at different potentials revealed an *e*-fold dependence with $\Delta V=-17.5$ mV (Figure 4a, dotted). These findings identified the voltage dependence and ion selectivity of $\alpha$-helical melittin as being similar to those of the asymmetric push–pull rod **5** in polarized SUVs (Figure 4a).

In clear contrast to melittin, gramicidin A caused equally rapid collapse both of $H^+$ and of $K^+$ gradients (Figure 4d). Moreover, almost voltage-independent $H^+/OH^-$-transport activity in spherical bilayers was found for gramicidin A (Figure 4b, open circles), as expected from conductance experiments in planar bilayers.[3] These findings identified the voltage dependence, but not the ion selectivity, of $\beta$-helical gramicidin A as similar to that of the symmetric push–push rod **6** in polarized EYPC-SUVs (Figure 4b).

The activity of push–pull rod **5** was further studied in polarized EYPC-SUVs ($V=-180$ mV) in the presence of different external anions $X^-$ and cations $M^{n+}$ (Figures 3c and 5). Replacement of external $Na^+$ by $Li^+$ or $Mg^{2+}$ did not affect the activity of push–pull $\beta$-barrel **5**[↑↑↑↑] as expected for anion selectivity (Figure 5b). The decrease in activity of **5** with external $I^- \geq Cl^- \geq OAc^- \geq F^-$ was similar to a Hofmeister or lyotropic anion selectivity sequence[13] (Figure 5a).

An increase in the fraction of negatively charged lipid EYPG in mixed EYPG/EYPC-SUVs with an inside-negative membrane potential of $V=-180$ mV gradually reduced the activity of push–pull rod **5** (Figure 6). The identical intensities of safranin O emission in anionic EYPC/EYPG-SUVs and in neutral EYPC-SUVs showed that this change did not originate from any influence of symmetric surface potentials

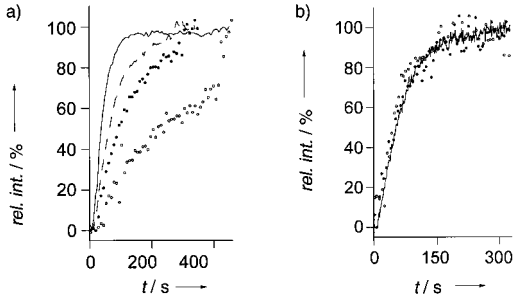


Figure 5. *p*-Octiphenyl **5** induced changes in emission intensity of HPTS in polarized EYPC-SUVs ($V=-180$ mV) in the presence of various external anions (a) and cations (b). External ions (decreasing activity) a): NaI (——), NaCl (- - - -), NaOAc (●), NaF (○), b): LiCl (——), NaCl (●), and $MgCl_2$ (○). For schematic presentation of the assay, see Figure 3c.

$\Psi_0$ on membrane potential *V*.[14] Before saturation, the activity of push–pull rod **5** in anionic vesicles roughly followed the fourth-power concentration dependence determined previously[8] in neutral EYPC-SUVs (Figure 6a). The monomer concentrations necessary to produce 50% pH-gradient collapse within 100 s ($c_M(50)$) increased exponentially with the surface potential $\Psi_0$ as calculated by the Gouy–Chapman theory (Figure 6b).

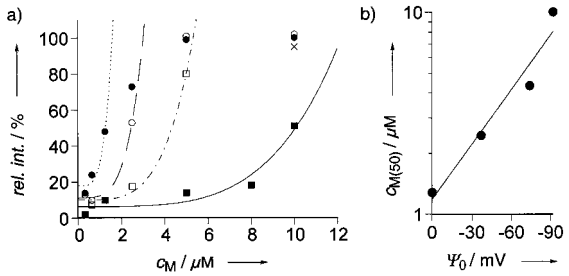


Figure 6. Activity of *p*-octiphenyl **5** with increasing surface potential $\Psi_0$ of polarized EYPC/EYPG-SUVs ($V=-180$ mV). a) Dependence of activity on the concentration of **5** in EYPC/EYPG-SUVs containing 0% (●), 10% (○), 30% (□) and 50% (■) of EYPG with fourth-power fit. b) $c_M(50)$ as a function of $\Psi_0$ with exponential curve fit.

**Activity of rigid push–pull $\beta$-barrels in planar EYPC bilayers:** The activity and selectivity of push–pull rod **5** in planar bilayers were studied by conventional BLM conductance experiments. (Note, positive input voltage corresponds to inside-negative Nernst potentials in EYPC-SUVs.) Application of a $+20$ mV s$^{-1}$ ramp after *cis*-addition of rigid push–pull rod **5** caused the appearance of exponentially increasing currents above $+100$ mV (Figure 7A). Whereas the average change in macroscopic current with increasing voltage was fully reproducible, the number and magnitude of discrete transitions between $+100$ and $+200$ mV changed from experiment to experiment (Figure 7a and b). A macroscopic *I*/*V* curve with minimal contributions from single-molecule events was used to illustrate an *e*-fold increase of the macroscopic current every $+26.4$ mV (Figure 7b).

Subsequent return from $+200$ mV to 0 mV with a $-20$ mV s$^{-1}$ ramp occasionally resulted in a roughly linear decrease in the macroscopic current (Figure 7B). Continuation to negative input voltage induced the disappearance of conductivity between $-50$ and $-150$ mV in discrete transi-

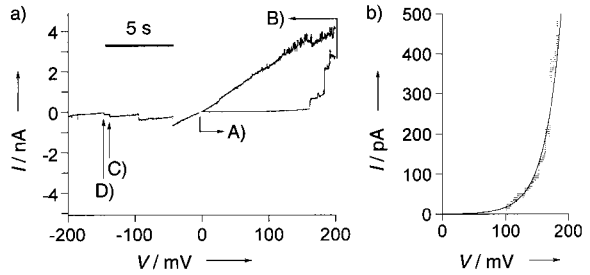


Figure 7. Macroscopic *I*/*V* characteristics of rigid push–pull rod **5** (1 μM) in EYPC-BLMs. a) +20 mV s$^{-1}$ ramp from A) 0 mV to +200 mV after *cis*-addition of **5** followed by one second at +200 mV and a −20 mV s$^{-1}$ ramp from B) +200 mV to −200 mV; C) discrete transition of 0.84 nS; D) discrete transition of 0.66 nS. b) +20 mV s$^{-1}$ ramp from 0 mV to +200 mV (••••) with exponential curve fit (——).

tions of various magnitude at inconstant voltage (Figure 7C and D). The two smallest observed transitions corresponded to single-channel conductances of 0.66 nS and 0.84 nS (compare Figure 8).

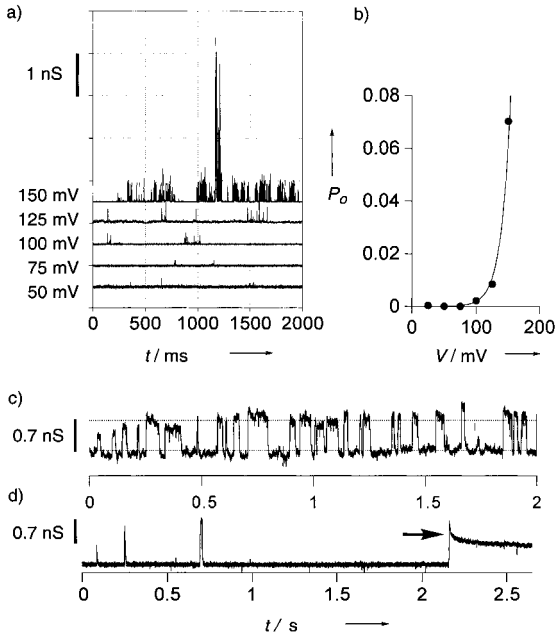


Figure 8. Single-channel characteristics of rigid push–pull rod **5** (1 μM *cis*) in EYPC-BLMs. a) Representative traces between +50 and +150 mV. b) $P_o/V$ curve with exponential fit. c) Illustrative trace for multi-level open states at +150 mV. d) Illustrative trace for apparent transition from short-lived to long-lived open states (arrow) at +100 mV.

Optimized experimental conditions were required to obtain macroscopic *I*/*V* curves with complete hysteresis, as in Figure 8a. Indicative of unfavorable formation of stable ion channels, it was observed that faster ramps and shorter resting times at $V = +200$ mV can result in reduced hysteresis. Higher rod concentrations and longer resting times at $V = +200$ mV, on the other hand, often caused membrane breakdown.

In single-channel experiments, short-lived multi-level currents were most frequently observed at high voltage (Figure 8). The open probability $P_o$ increased steeply in *e*-fold every +14.4 mV (Figure 8b). The conductance levels of these short-lived channels (Figure 8a and c) ranged between 0.4 and 0.9 nS, except for occasional bursts at high potential. Although infrequent, opening of long-lived single channels could be detected (0.7 nS). Its unusual shape, a high-conductance burst as shown in Figure 8a, followed by a slow decrease, suggested that the formation of long-lived channels occurs through unstable pores (Figure 8d).

The ion selectivity of rigid push–pull rods **5** was studied in EYPC-BLMs by conventional methods based on the application of salt gradients between the *cis* and the *trans* chamber (Table 1). Reversal potentials $V_r$ obtained under various KCl gradients were consistent with anion selectivity of **5**. Permeability ratios ($P_{Cl^-}/P_{K^+}$) of between 2.7 to 3.7 were calculated by use of the GHK equation (see Experimental Section). Weak $Cl^- > OAc^-$ selectivity was indicated by $P_{Cl^-}/P_{OAc^-} = 1.8$ obtained from a positive $V_r$ with *trans*-NaOAc. Almost negligible $F^- \geq OAc^-$ selectivity was indicated by $P_{Cl^-}/P_{F^-} = 1.3$. Multichannel conductance experiments thus revealed an overall selectivity sequence $Cl^- \geq F^- \geq OAc^- > K^+$.

Table 1. Ion selectivity of rigid push–pull rod **5** in EYPC-BLMs.

| *cis* | *c* [M] | *trans* | *c* [M] | $V_r$ | $P_{Cl^-}/P_{K^+/A^-}$ |
|---|---|---|---|---|---|
| KCl | 1.0 | KCl | 0.5 | +7.1 | 2.7[a] |
| KCl | 1.0 | KCl | 0.25 | +14.4 | 3.0[a] |
| KCl | 0.1 | KCl | 1.0 | −25.3 | 3.7[a] |
| NaCl | 1.0 | NaOAc | 1.0 | +10.7 | 1.8[b] |
| NaCl | 0.5 | NaF | 0.5 | +7.8 | 1.3[c] |

[a] $P_{Cl^-}/P_{K^+}$. [b] $P_{Cl^-}/P_{OAc^-}$. [c] $P_{Cl^-}/P_{F^-}$.

**Activity of symmetric rigid-rod β-barrels in planar EYPC bilayers:** The activity of push–push rod **6** was studied in planar bilayers under the conditions used for push–pull rod **5**. Macroscopic *I*/*V* curves showed a nearly linear *I*/*V* relationship with very weak hysteresis at high voltage (Figure 9a). Open channels showed almost infinite lifetime within ±170 mV. Rare single-channel current transitions were only observed above this critical voltage of $V = \pm 170$ mV (Figure 9b). The single-channel conductance was comparable to that of long-lived channels seen for asymmetric rod **5** in multichannel (Figure 7C and D) and occasionally also in single-channel experiments (Figure 8d).

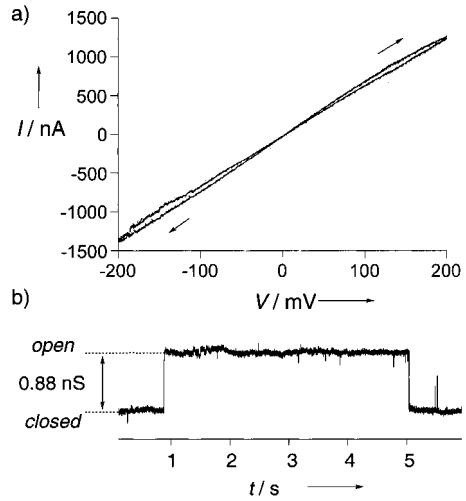


Figure 9. Macroscopic *I*/*V* curve and single-channel characteristics of rigid push–push rod **6** (5 μM *cis*) in EYPC-BLMs. a) Representative 20 mV s$^{-1}$ ramps, arrows indicate ramps from 0 to high voltage. b) Single-channel trace at +200 mV.


© 2003 WILEY-VCH Verlag GmbH & Co. KGaA, Weinheim
0947-6539/03/0901-0226 $ 20.00+.50/0 *Chem. Eur. J.* **2003**, *9*, No. 1

**Fluorescence depth quenching and circular dichroism:** Noninvasive FDQ experiments with ion channels **5** and **6** are greatly simplified by the intense blue fluorescence of the entire *p*-octiphenyl rod.[4] Previous studies have implied that two spin-labeled EYPC-SUVs containing either 12-DOXYL-quenchers $Q_1$ near the middle or interfacial 5-DOXYL-quenchers $Q_2$ are sufficient for study of the partitioning and orientation of *p*-octiphenyl fluorophores in lipid bilayers under conditions relevant for activity. Comparison of the quenching efficiency of central $Q_1$ and interfacial $Q_2$ with the *p*-octiphenyl emission in unlabeled EYPC-SUVs allows qualitative differentiation between central ($Q_1 > Q_2$ efficiency), interfacial ($Q_1 < Q_2$), and TM rod orientation ($Q_1 \approx Q_2$).

At monomer concentrations $c_M = 250$ nM, relatively poor $Q_1 \approx Q_2$ 23% quenching was observed with push–pull rod **5** in spherical bilayers with (filled symbols) and without (open symbols) inside-negative membrane potential (Figure 10b). Increasing monomer concentration resulted in increased efficiency of central $Q_1$ (filled circles) but not interfacial $Q_2$ (filled squares) in polarized membranes. At higher concentrations, the same effect was seen in unpolarized membranes. Interestingly, symmetric push–push rod **6** showed consistently weaker partitioning with polarized spherical EYPC-SUVs than with unpolarized spherical EYPC-SUVs (Figure 10c). With increasing concentration of **6**, a shift in relative efficiency from ($Q_1 \approx Q_2$)- toward ($Q_1 > Q_2$)-FDQ was observed, similar to that seen with asymmetric **5**.

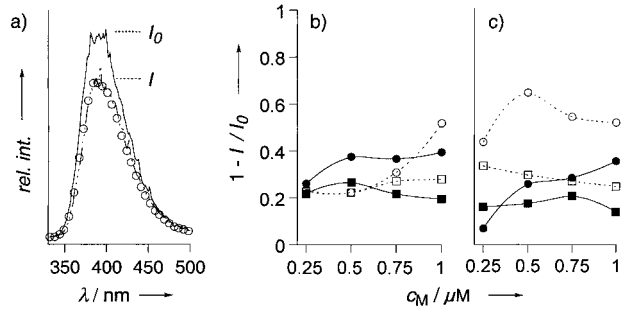


Figure 10. a) Emission spectra of push–pull rod **5** (500 nM, $\lambda_{exc}$ 320 nm) in the presence of unlabeled EYPC-SUVs ($I_0$, solid) and EYPC-SUVs doped either with 8.9 mol% 5-DOXYL-PC ($I$, dashed) or with 12-DOXYL-PC ($I$, open circles) at $V = 0$ mV. b) Change in quenching efficiency $1 - I/I_0$ with increasing concentration of push–pull **5** with 5-DOXYL-PC (squares) and 12-DOXYL-PC (circles) at $V = 0$ mV (open symbols) and $V = -180$ mV (filled symbols). c) As in (b) for push–push rod **6**.

The same influence of membrane potentials on partitioning was observed by CD spectroscopy. In buffer, the CD spectra of push–pull and push–push rods **5** and **6** each exhibited a strong positive first Cotton effect around 340 nm (Figure 11a, solid). Originating from low-energy $L_a$ transitions in the chiral *p*-octiphenyl chromophore, the precise structural basis of this effect is unknown. The existence of rigid-rod $\beta$-barrels **5** and **6** in water can thus be excluded not only as judged from the non-linear dependence of activity on $c_M$,[8] but also because *p*-octiphenyl $\beta$-barrels usually give negative first Cotton effects at 300–330 nm.[15] Such negative first Cotton effects at 310 nm, of very small magnitude, indeed remained after the addition of an excess of polarized and unpolarized

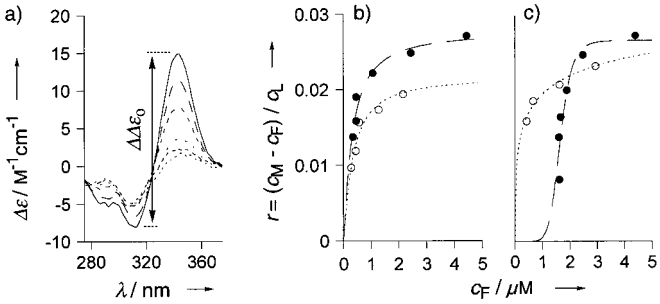


Figure 11. a) CD spectra of push–pull rod **5** (10 μM) in the presence of increasing concentrations of unpolarized EYPC-SUVs (0 mM: ——, 1.65 mM EYPC: ••••). b) CD-partitioning isotherms of **5** at $V = 0$ mV (○) and $V = -180$ mV (●). c) As in (b) for push–push rod **6**.

EYPC-SUVs, while the strong positive CD Cotton effect at 340 nm nearly vanished (Figure 11a, dotted).

Partitioning isotherms were derived from the changes in "amplitude" $\Delta\Delta\varepsilon$ of the bisignate low-energy CD Cotton effects of push–pull rods **5** induced by EYPC-bilayers (see Experimental Section). The $r/c_F$ curves corroborated the preferential partitioning of **5** to polarized relative to unpolarized EYPC-SUVs indicated by FDQ (Figure 11b, filled versus open circles). From the initial slope, apparent partition coefficients $\Gamma = 3.8 \times 10^4\,M^{-1}$ and $\Gamma = 2.8 \times 10^4\,M^{-1}$ were calculated at $V = -180$ mV and $V = 0$ mV, respectively. Clearly, the partition coefficients $\Gamma$ decreased in both situations with increasing concentration of free push–pull rod **5**.

Similar CD isotherms were obtained for push–push rod **6** ($\Gamma = 3.1 \times 10^4\,M^{-1}$) in unpolarized EYPC-SUVs (Figure 11b versus c, open circles). As observed with FDQ, partitioning of push–push rod **6** at low concentrations became highly unfavorable upon application of an inside-negative membrane potential (Figure 11c, filled versus open circles).

## Discussion

**Planar versus spherical bilayers:**[16] The ion channel characteristics of push–pull rod **5** and control molecules obtained with planar and spherical bilayer membranes are summarized in Table 2. In EYPC-BLMs, voltage-dependent ion-channel formation, expressed as $z_g = 0.96$, was observed in macroscopic $I/V$ curves in the presence of push–pull rod **5** (Figure 7). In single-channel experiments, this characteristic was well reflected in the exponential increase in open probability (Figure 8b), while current rectification[2a, 5b] was

Table 2. Summary of results in SUVs and BLMs.

| Compound | $z_g$ BLM | $z_g$ SUV | Ion selectivity BLM | Ion selectivity SUV |
|---|---|---|---|---|
| **5** | 0.96,[a] 1.75[b] | 0.85[c] | $Cl^- \geq F^- > M^+$[d] | $Cl^- > F^- > M^+$[e] |
| melittin | 0.95,[f] 1.2,[g] 4[h] | 1.50[c] | $A^- > M^+$[f] | $Cl^- > M^+$[c] |
| **6** | ohmic[i] | ohmic[c] | n.d. | $Cl^- > M^+$[j] |
| gA[k] | ohmic[l] | ohmic[c] | $M^+ > A^-$[l] | $M^+ > Cl^-$[c] |

[a] Multichannel $I(V)$, Figure 7b. [b] Single-channel $P_o(V)$, Figure 8b. [c] Figure 4. [d] Table 1. [e] Figure 5. [f] Ref. [1b]. [g] Ref. [9b]. [h] Ref. [9f]. [i] Figure 9a. [j] Same as **5**,[8] **6** caused rapid collapse of pH gradient before $K^+$ concentration gradient (not shown). [k] gA = Gramicidin A. [l] Ref. [3a].

 © 2003 WILEY-VCH Verlag GmbH & Co. KGaA, Weinheim 0947-6539/03/0901-0227 $ 20.00+.50/0 

not evident. The difference in gating charges found in macroscopic $I/V$ and single-channel $P_o/V$ curves probably originated from difficulties in the accurate determination of low open probabilities.

In contrast to BLM-conductance experiments, studies on voltage dependence and ion selectivity in SUVs/LUVs are rare[11, 12b] and sometimes under-appreciated.[2c] The results obtained both on the voltage dependence and on the ion selectivity of **5** in SUVs were, however, in quantitative agreement with those from BLM experiments (Table 2).[16] Qualitative trends for anion/cation selectivity in spherical bilayers could already be secured by the same fluorimetric assay as used to determine potential dependence (Figure 4). Namely, both the push–pull rod **5** and the anion-selective melittin induced faster collapse of $OH^-/H^+$ than $K^+$ gradients, while cation-selective gramicidin A caused simultaneous decay of pH and $K^+$ gradients (Table 2). The implied anion selectivity for **5** was corroborated by the influence of external anions and cations on flux rates (Figures 3c and 5). The results with different external anions, consistently with insights from BLMs (Table 1), indicated a weakly lyotropic selectivity sequence of push–pull rod **5** in SUVs (Figure 5a). Whereas the anion selectivity of ion channels formed by **5** in SUVs and BLMs was as expected for polycationic pores, a lyotropic selectivity sequence was more surprising because it implied anion dehydration (i.e., anion binding to the ammonium cations of **5**) during transmembrane translocation.

The validity of the above studies with push–pull rod **5** in polarized SUVs is supported by various results beyond melittin. For instance, the voltage independence observed in SUVs for the anion selective, symmetric rod **6**[8] was confirmed by BLM experiments (Figure 9a) and by comparison with gramicidin A (Figure 4b). Moreover, the consistent voltage dependence of cation-selective tetraazacrown-*p*-octiphenyls **3**[6a] and hexaazacrown-*p*-octiphenyls **4**,[6b] as well as the special situation with proton transporters in polarized SUVs,[17] have been discussed previously. The overall excellent agreement found between results on voltage dependence and ion selectivity in BLMs and SUVs is not trivial[2c] and of great interest because of the marvelous complementarity of the two model systems.[16] Namely, BLMs provide access to ion channel characteristics on the macroscopic and especially the single-molecule levels, whereas SUVs/LUVs are directly compatible with the structural and thermodynamic studies required to rationalize function.

**Asymmetric versus symmetric rigid-rod $\beta$-barrels:** In rigid-rod molecules **5** and **6**, 491 out of 492–494 atoms—or 99.4–99.8% of all atoms—are identical (Figure 2). Their activities in planar and spherical lipid bilayers, however, differ dramatically. This difference is of particular significance. It demonstrates the importance of the axial dipole not only for the recognition of polarized membranes but also for the stability of the supramolecular assembly.

*Push–push rod* ***6***: In BLMs, symmetric push–push rod **6** formed stable and large ohmic ion channels compatible with rigid-rod $\beta$-barrel $\mathbf{6}^{\text{IIII}}$ (Figures 9 and 12). The remarkable stability of tetramer $\mathbf{6}^{\text{IIII}}$ was comparable to that reported previously for hexameric rigid-rod $\beta$-barrel $\mathbf{7}^{\text{IIIIII}}$ (Figure 12).[7a] This similarity suggested that removal of the terminal peptide strands in symmetric *p*-octiphenyl $\beta$-barrel $\mathbf{7}^{\text{IIIIII}}$ does not reduce barrel stability. However, the single-channel conductance of push–push barrel $\mathbf{6}^{\text{IIII}}$ was similar to that

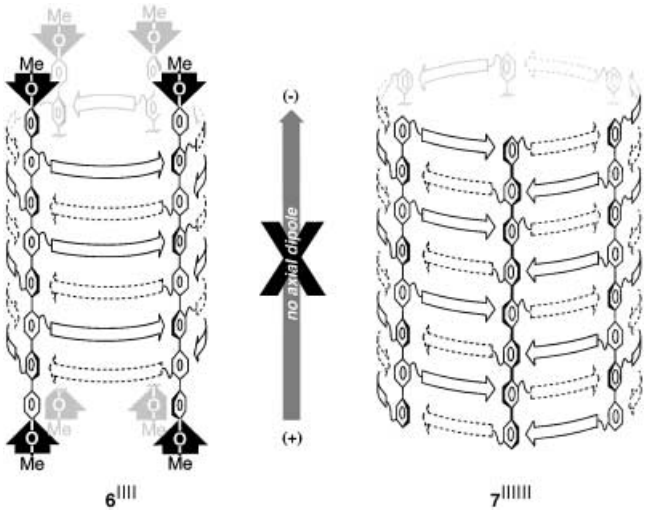


Figure 12. Putative suprastructures of symmetric $\beta$-barrels $\mathbf{6}^{\text{IIII}}$ and $\mathbf{7}^{\text{IIIIII}}$ (symbols as in Figure 2); see ref. [7] for details on barrel $\mathbf{7}^{\text{IIIIII}}$.

of push–pull barrel $\mathbf{5}^{\uparrow\uparrow\uparrow\uparrow}$ and thus indicative of a tetrameric suprastructure characterized by fourth-power dependence of activity on monomer concentration[8] rather than a hexamer such as $\mathbf{7}^{\text{IIIIII}}$ with sixth-power dependence on $c_M$ and much higher single-channel conductance.[7a] This suggested that formal removal of two terminal peptide strands in hexamer $\mathbf{7}^{\text{IIIIII}}$ causes contraction to tetramer $\mathbf{6}^{\text{IIII}}$. One plausible origin of this barrel contraction is the reduction of the number of protonated internal amines of lysine side chains at pH 7.[18] A more detailed analysis of the overall poorly understood interdependence of internal charge repulsion, $pK_a$ values, counterion effects, and stability of *p*-octiphenyl $\beta$-barrels with internal aspartates,[19] histidines,[20] and lysines[7a, 8] is reported elsewhere.[21]

Ohmic behavior of *p*-octiphenyl $\beta$-barrels $\mathbf{6}^{\text{IIII}}$ was as expected from uniform distribution of charges and nullified amide dipoles in a $\beta$-sheet conformation. The weak hysteresis in the multichannel $I/V$ curves and the reduced stability in single-channel experiments at $V = +200$ mV suggested that the formation of "dipole-free" ion channels $\mathbf{6}^{\text{IIII}}$ (i.e., the formation of $\beta$-sheets) may be hindered at high voltage (Figure 9). Experimental support for this speculation was secured by structural studies in SUVs. Both CD and FDQ isotherms demonstrated that partitioning of push–pull rods **6** to EYPC bilayers is strongly reduced by inside-negative potentials at $c_M$, $c_F < 1\,\mu$M (Figures 10c and 11c). Only very weak partitioning of rod **6** at the membrane/water interface of polarized SUVs remained at $c_M = 250$ nM (Figure 10c, filled squares).

*Push–pull rod* ***5***: In sharp contrast to symmetric *p*-octiphenyl **6**, ion-channel formation by push–pull rod **5** was voltage-dependent in BLMs and SUVs (Table 2). Transient, multi-


© 2003 WILEY-VCH Verlag GmbH & Co. KGaA, Weinheim
0947-6539/03/0901-0228 $ 20.00+.50/0 *Chem. Eur. J.* **2003**, *9*, No. 1

level ion channels (Figure 8a, c) as well as stable, ohmic ion channels (Figures 7B and 8d) were observed. With the exception of occasional bursts with the former (Figure 8a), channel conductances were in the range of 0.4–0.9 nS.

Interpretation of the stable channels as parallel $\beta$-barrels $\mathbf{5}^{\uparrow\uparrow\uparrow\uparrow}$ was acceptable for the following reasons (Figures 2 and 13). High stability and nearly voltage-independent conductance were consistent with interdigitating $\beta$-sheets. These channels formed only at high membrane potentials, which would orient the axial macrodipoles of monomeric push–pull rods parallel to each other despite dipole–dipole repulsion. Overall electrostatic asymmetry of $\beta$-barrels $\mathbf{5}^{\uparrow\uparrow\uparrow\uparrow}$ was evident as these channels remained open in the presence of constructive dipole–potential interaction (Figure 7B) and closed with increasingly destructive dipole–potential interaction (Figure 7C, D).

Judged from their similar single-channel conductances, the transient channels observed with push–pull rod **5** may represent precursors of parallel $\beta$-barrels $\mathbf{5}^{\uparrow\uparrow\uparrow\uparrow}$ (Figure 13). Reminiscent of $\alpha$-helix bundles (see below), these $\alpha_{lk}$-barrels $\mathbf{5}^{\uparrow\sim\uparrow\sim\uparrow\sim\uparrow}$ may be imagined as bundles of parallel TM-rods that lack stabilization from interdigitating $\beta$-sheets in $\beta$-barrels $\mathbf{5}^{\uparrow\uparrow\uparrow\uparrow}$. The initial current decrease during the transition from single transient $\alpha_{lk}$-barrels $\mathbf{5}^{\uparrow\sim\uparrow\sim\uparrow\sim\uparrow}$ to single stable $\beta$-barrels $\mathbf{5}^{\uparrow\uparrow\uparrow\uparrow}$ would then report multiple, slow conformational changes during peptide interdigitation and $\beta$-sheet formation on the single-molecule level (Figure 8d, arrow).[22]

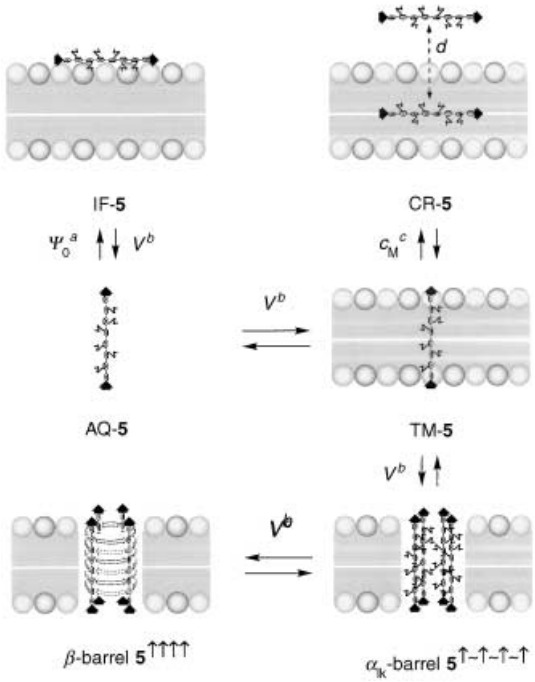


Figure 13. Working hypothesis for the action of push–pull rod **5** at low $c_M$ as a function of increasing membrane potential ($V$), surface potential ($\Psi_0$), and monomer concentration ($c_M$). a) Not verified; b) opposite for push–push rod **6**; c) identical for push–push rod **6**; d) minimized charge repulsion between membrane-bound **5** and excess AQ-**5** (TM: transmembrane, IF: interfacial, CR: central, AQ: aqueous; conformation and aggregation numbers $n$ are unknown except for $\mathbf{5}^{\uparrow\uparrow\uparrow\uparrow}$ and $n=1$ for TM-**5**/CR-**5**).

On the structural level, both CD and FDQ isotherms demonstrated that partitioning of push–pull rods **5** to EYPC-SUVs is facilitated by membrane polarization, particularly at $c_M$, $c_F < 1\ \mu M$ (Figures 10b and 11b). Opposite trends for symmetric rods **6** (Figures 10c and 11c) supported the view that dipole–potential interaction is more significant than fixed positive charges for the recognition of polarized membranes.[23] The resulting increase in concentration of the push–pull rod in polarized bilayers appears to account mainly for voltage dependence.[10]

Stabilization of TM rod orientation[24, 25] by dipole–potential interaction was not observed directly by FDQ, because the orientation of asymmetric **5** at low concentrations is TM with and without membrane potential (Figure 10b). However, dipole–potential interactions did prevent the reorientation from TM-**5** to IF-**5** (and AQ-**5**) during membrane polarization at low concentrations that was observed with push–push rod **6** (Figure 13). An increase in $c_M$ reduced the partition coefficient $\Gamma$ (Figure 11) and caused rod accumulation in the center of bilayers with and without membrane potential (Figure 10). Both effects can be explained in terms of increasing charge repulsion between membrane-bound and free polycationic rods at elevated concentration (Figure 13).

The mechanism of deactivation of push–pull rod **5** by surface potentials was not studied on the structural level. It can be rationalized either by stronger interfacial binding along $\Psi_0$ rather than $V$ (Figure 13), by reduced anion concentration in the vicinity of the channels, or by a combination of both effects. A summary of all above trends from structural and functional studies in SUVs and BLMs is made in the hypothetical mechanism in Figure 13.

***p*-Octiphenyl $\beta$-barrels versus natural $\alpha$- and $\beta$-barrels:** The characteristics of ion channels formed by symmetric rigid-rod $\beta$-barrels such as tetramer $\mathbf{6}^{|||}$ or $\mathbf{7}^{|||||}$ are similar to those formed by natural $\beta$-barrels such as porins, $\alpha$-toxin, and aerolysin:[26] high stability, large diameter, ohmic behavior at low voltage, and destabilization by high voltage. Given the unresolved difficulties in de novo synthesis of $\beta$-barrels, symmetric rigid-rod $\beta$-barrels therefore offer unique, facile, and versatile access to these desirable ion-channel properties. The key advantage of $\beta$-barrels over, for example, $\beta$-helical ion channels such as gramicidin A for practical applications, the precise positioning of variable functional groups along a large central channel,[27] is preserved in synthetic *p*-octiphenyl $\beta$-barrels.

Voltage-dependent formation of short-lived, multi-level single ion channels, on the other hand, is characteristic for some neutral and many cationic, transient, presumably toroidal[28] "$\alpha$-barrels" and other asymmetric scaffolds. Examples include melittin,[9e] retromelittin,[9a] magainin 2,[29] trichotoxins,[9e] oligo(Ala-Aib-Ala-Aib-Ala)s,[2c] asymmetric gramicidin,[3a] and synthetic bolaamphiphiles.[5a] Further similarities between polycationic rigid-rod $\alpha_{lk}$-barrel $\mathbf{5}^{\uparrow\sim\uparrow\sim\uparrow\sim\uparrow}$ and melittin include gating charge and anion selectivity (Table 2), decreasing partition coefficient $\Gamma$ with increasing monomer concentration,[9c] thermodynamically unfavorable self-assembly,[9d] and decreasing activity with increasing $\Psi_0$.[30] The differences between rigid-rod $\alpha_{lk}$-barrel $\mathbf{5}^{\uparrow\sim\uparrow\sim\uparrow\sim\uparrow}$ and natural

$\alpha$-barrels, however, may be even more interesting: the voltage-dependent self-assembly of transient $\alpha_{lk}$-barrels $\mathbf{5}^{\uparrow\sim\uparrow\sim\uparrow}$ can evolve to stable, oriented, parallel rigid-rod $\beta$-barrels $\mathbf{5}^{\uparrow\uparrow\uparrow\uparrow}$ (Figure 13). Also unlike $\alpha$-helical dipoles, the axial dipole moment of rigid, fluorescent *p*-octiphenyl rods is not subject to conformational isomerization but can be chemically "switched off" without global structural change.[4] In other words, transition from $\alpha$-barrel- to $\beta$-barrel-like ion channels is possible in the context of the same structural motif, either in situ ($\mathbf{5}^{\uparrow\sim\uparrow\sim\uparrow\sim\uparrow}$ versus $\mathbf{5}^{\uparrow\uparrow\uparrow\uparrow}$) or by extremely small chemical modifications ($\mathbf{5}^{\uparrow\sim\uparrow\sim\uparrow\sim\uparrow}$ versus $\mathbf{6}^{\text{IIII}}$).

## Conclusion

In planar and spherical lipid bilayers, parallel self-assembly of transmembrane push–pull *p*-octiphenyls **5** into transient "$\alpha_{lk}$-barrel" and stable $\beta$-barrel anion channels with large interiors ($g \approx 0.7$ nS) is facilitated by membrane potentials ($z_g = 0.85$–1.75) and hindered by surface potentials. The characteristics of $\alpha_{lk}$-barrels $\mathbf{5}^{\uparrow\sim\uparrow\sim\uparrow\sim\uparrow}$ are similar to those of "$\alpha$-barrel" ion channels formed by cationic $\alpha$-helical peptides including several natural antibiotics. Unlike biological "$\alpha$-barrels", however, this voltage-dependent self-assembly a) occurs from rigid fluorescent rods and b) can continue to afford stable ion channels $\mathbf{5}^{\uparrow\uparrow\uparrow\uparrow}$ with similarities to symmetric >99%-homologous $\mathbf{6}^{\text{IIII}}$ and biological $\beta$-barrels such as porins. We conclude that a single synthetic suprastructural motif made from abiotic *p*-octiphenyl rods can be tuned to exhibit the complementary characteristics of biological $\alpha$-barrel and $\beta$-barrel ion channels either temporarily or permanently.

## Experimental Section

**Materials**: The syntheses and characterization of $1^4$-methoxy-$8^4$-methylsulfonyl-$2^2$,$3^3$,$4^2$,$5^3$,$6^2$,$7^3$-hexakis(Gla-Leu-Lys-Leu-$NH_2$)-*p*-octiphenyl (**5**) and $1^4$,$8^4$-bismethoxy-$2^2$,$3^3$,$4^2$,$5^3$,$6^2$,$7^3$-hexakis(Gla-Leu-Lys-Leu-$NH_2$)-*p*-octiphenyl (**6**) were as described.[8] EYPC and EYPG were purchased from Northern Lipids Inc. (Vancouver, British Columbia, Canada), 5-DOXYL-PC and 12-DOXYL-PC from Avanti Polar Lipids (Alabaster, AL), HPTS from Molecular Probes (Eugene, OR), gramicidin A from Calbiochem–Novabiochem (San Diego, CA), and melittin, valinomycin, safranin O, detergents, all salts and buffers of the best grade available from Sigma–Aldrich Corp. (St. Louis, MO), and used as received.

**Vesicle experiments**: Fluorescence spectra were recorded in 1.0 cm cells on FluoroMax-2 (Jobin Yvon Inc., Edison, NJ) equipped with an injector port, a stirrer, and a temperature controller (25 °C), CD spectra on a JASCO-710 spectropolarimeter (JASCO Corp., Tokyo, Japan) equipped with a stirrer and a temperature controller (23 °C).

**Vesicle preparation**: Uniformly sized (ca. 68 nm) EYPC-SUVs were prepared by the dialytic cholate removal method as described previously (Supporting Information of ref. [8] and references therein). The interior of the resulting EYPC-SUVs (10 mM EYPC) contained 90 μM HPTS, 100 mM KCl, and 10 mM $K_mH_nPO_4$, pH 6.4, the exterior 100 mM NaCl and 10 mM $Na_mH_nPO_4$, pH 6.4. Mixed EYPC/EYPG-SUVs and DOXYL-labeled EYPC-SUVs were prepared identically from the corresponding mixtures of EYPC and either EYPG or 5-/12-DOXYL-PC.

**Vesicle polarization**: EYPC-, EYPC/EYPG-, and DOXYL-PC/EYPC-SUVs were polarized as described for EYPC-SUVs.[8] The method for vesicle polarization and depolarization is schematically summarized in Figure 3. In brief, 50 μL of SUV stock solution (10 mM, final conc. 0.25 mM) were diluted with 1.95 mL of a mixture of *n* mL of 100 mM NaCl, 10 mM $Na_mH_nPO_4$, pH 6.4, and *k* μL of 100 mM KCl, 10 mM $K_mH_nPO_4$, pH 6.4, containing safranin O (6 nM). By assuming external $[K^+_{out}] \approx 0$ in the SUV stock solution, *n* and *k* were calculated from the Nernst equation for $K^+$:

$$V\,[\text{mV}] = 59 \times \log(c_{\text{Kout}}/c_{\text{Kin}}) \quad (1)$$

giving:

$V = -180$ mV: $n = 1.95$ mL, $k = 1.8$ μL,
$V = -160$ mV: $n = 1.95$ mL, $k = 3.9$ μL,
$V = -150$ mV: $n = 1.95$ mL, $k = 5.7$ μL,
$V = -140$ mV: $n = 1.94$ mL, $k = 8.5$ μL,
$V = -100$ mV: $n = 1.91$ mL, $k = 40.4$ μL,
$V = -50$ mV: $n = 1.72$ mL, $k = 284$ μL,

and so on. The emission of safranin O was monitored at 581 nm ($\lambda_{exc}$ 522 nm) during addition of base (20 μL of 0.5 M NaOH, final 5 mM) and valinomycin (20 μL of 60 μM, final 0.6 μM). After the addition of valinomycin, gradual build-up of membrane potential was reflected in the increase of safranin O emission intensity until saturation was reached within ≈100 s. The resulting emission intensity was compared with the calibration curve to verify the applied membrane potential. The calibration curve was obtained by plotting the observed fluorescence intensity (intensity × volume) after successive addition of external $K^+$ buffer against the calculated Nernst potential. Linear correlation was found between −40 and −160 mV.[8, 12a] Extrapolation to $k = 0$, $n = 1.95$ mL gave $V = -190$ mV: inconsistency with the expected Nernst potential ($-\infty$ mV) may originate from residual external $K^+$ in the SUV stock solution or be due to "saturation".[12a] According to the safranin O emission, the symmetric surface potentials in EYPC/EYPG-SUVs[14] did not affect the apparent membrane potential. To assess ion selectivities (see below), external NaCl in sodium phosphate buffer was replaced by LiCl, $MgCl_2$, NaOAc, NaI, or NaF.

**Ion transport in polarized vesicles**: Transport experiments were initiated by addition of samples (20 μL of stock solutions, **5**: 0.01–1 mM in MeOH, final 0.1–10 μM; melittin: 2 μM in water, final 20 nM; gramicidin A: 20 μM in DMSO, final 0.2 μM) to polarized SUVs (prepared as above) and terminated by addition of excess melittin (20 μL of 0.1 mM). Changes in fluorescence intensities of safranin O ($\lambda_{exc}$ 522 nm, $\lambda_{em}$ 581 nm) and HPTS ($I_{a1}$: $\lambda_{exc}$ 405 nm, $\lambda_{em}$ 510 nm; $I_{a2}$: $\lambda_{exc}$ 450 nm, $\lambda_{em}$ 510 nm) were simultaneously monitored as a function of time during the SUV polarization and transport experiment. Precise control of temperature and continuous stirring during fluorescence kinetics measurements were crucial for reproducible results.

To minimize the artifactual variations, curves obtained for HPTS channels were first subjected to ratiometric calibration ($I_t = I_{a2}/I_{a1}$) and then normalized by use of

$$I_n[\%] = (I_t - I_0)/(I_\infty - I_0) \times 100 \quad (2)$$

where $I_0$ is $I_t$ right before sample addition and $I_\infty$ is $I_t$ after the addition of excess melittin. Normalized baselines were obtained by the same treatment of data obtained for each membrane potential without addition of the samples, and were subtracted from $I_n$ to give comparable data ($I_{rel}$). Dependence on membrane potential was expressed in $I_{100} - V$ curves and analyzed by exponential and linear curve fit for non-ohmic and ohmic behavior, respectively ($I_{100}$ is $I_{rel}$ 100 s after sample addition). Gating charges $z_g$ were calculated by use of

$$G_{vd} \propto c_M^n \exp(z_g e V/k T) \quad (3)$$

where $G_{vd}$ is the observed activity at $I_{100}$, $c_M$ is the monomer concentration, *n* the number of monomers in an active pore, *e* the elementary charge, *k* the Boltzmann constant, and *T* the absolute temperature.[2c] Dependence on surface potential was expressed in $I_{100} - \Psi_0$ curves. Surface potentials $\Psi_0$ were calculated by use of the Gouy–Chapman equation:

$$\sigma^2 = 2000\,\varepsilon_0 \varepsilon_R R T \Sigma c_i [\exp(z_i F \Psi_0/R T) - 1] \quad (4)$$

where $\varepsilon_0$ is the permittivity of free space, $\varepsilon_R$ is the dielectric constant of the media (=78), *R* the gas constant, *T* the absolute temperature, $c_i$ and $z_i$ the


© 2003 WILEY-VCH Verlag GmbH & Co. KGaA, Weinheim
0947-6539/03/0901-0230 $ 20.00+.50/0 *Chem. Eur. J.* **2003**, *9*, No. 1

concentration (M) and charge of the *i*-th electrolyte, $F$ the Faraday constant, and σ the charge density approximated by Equation (5)

$$\sigma = -e x_{PG}(1 - x_{Na})/A_L \quad (5)$$

where $e$ is the elementary charge, $x_{PG}$ the mole fraction of EYPG, $x_{Na}$ the molar ratio of bound $Na^+$/lipid (0.6 $c_{Na}$), and $A_L$ the lipid surface area (68 Å$^2$).[31]

**Ion selectivity**: Information on anion/cation selectivity could be extracted from the triple-channel fluorescence kinetics described above with doubly-labeled polarized EYPC-SUVs, by taking account of the following:

Anion-selective pores:

1) pH gradients collapse more rapidly than $K^+$ gradients through fast $OH^-$/$Cl^-$ antiport (Figure 3a).
2) Replacement of external NaCl by MCl (M ≠ K) does not affect transport rates.
3) Replacement of external NaCl by NaX affects transport rates (Figure 3c).

Cation-selective pores:

1) pH gradients collapse either simultaneously with or more slowly than $K^+$ gradients (contributions from valinomycin) through $K^+$ or $H^+$/$Na^+$ antiport (Figure 3b).
2) Replacement of external NaCl by MCl (M ≠ K) affects transport rates.
3) Replacement of external NaCl by NaX does not affect transport rates; experimental procedure as above.

**Fluorescence depth quenching**: As described in ref. [6b], 5- or 12-DOXYL-PC/EYPC-SUVs (*w*/*w* 1:9) were prepared and polarized under conditions used for transport experiments (see above). Emission intensities ($I$, $\lambda_{exc}$ at 320 nm) of **5**/**6** (0.25–1 μM) in DOXYL-PC/EYPC-SUVs (0.25 mM) were compared to those in EYPC-SUVs ($I_0$) and expressed as quenching efficiencies ($1 - I/I_0$).

**CD Spectroscopy**: CD Spectra of **5**/**6** (10 μM) were recorded with increasing concentrations of EYPC-SUVs prepared and polarized as above. Δε values refer to total *p*-oligophenyl concentration ($c_M$), $c_L$ to total lipid concentration. Changes in CD "amplitude" $\Delta\Delta\varepsilon = \Delta\varepsilon_{max}{}^1$ (at ≈340 nm) − $\Delta\varepsilon_{max}{}^2$ (at ≈310 nm) with increasing lipid/rod molar ratio ($c_L/c_M$) were analyzed in $r/c_F$ curves by Equations (6) and (7):

$$r = \Gamma c_F \quad (6)$$

where $\Gamma$ is the partition coefficient, $r = (c_M - c_F)/c_L$,[9d] and

$$c_F = c_M(\Delta\Delta\varepsilon - \Delta\Delta\varepsilon_\infty)/(\Delta\Delta\varepsilon_0 - \Delta\Delta\varepsilon_\infty) \quad (7)$$

with $\Delta\Delta\varepsilon_\infty$ as amplitude for saturation and $\Delta\Delta\varepsilon_0$ as amplitude in the absence of SUVs.

**Planar bilayer experiments**: BLMs were formed by painting a solution of EYPC in *n*-decane (42 mg mL$^{-1}$) on an aperture ($d$ = 150 μm, pretreated with the same solution) in a delrin cuvette separating two chambers containing 1 mL each of 1M KCl and agar bridge connection (1M KCl) to Ag/AgCl electrodes (Warner Instrument Corp. Hamden, CT). Currents were recorded at different holding potentials (*trans* at ground) in a custom-made Faraday cage, amplified (BC-525c, Warner Instrument Corp.), low-pass filtered with an 8-pole Bessel filter at 5 kHz (LPF-8, Warner Instrument Corp.), A-D converted (Digipack 1200-2, Axon Instruments, Union City, CA), and sampled at 10 kHz by computer (pClamp 8.0, Axon Instruments). Samples were added to the *cis* chamber. All the conductance measurements were performed at room temperature (22 ± 1 °C). The overall reliability of the employed system was regularly assessed by use of alamethicin as a model channel. The conductances of multilevel channels and voltage dependence were fully reproducible and consistent with the literature.[32]

The salt gradients applied to determine ion selectivities are summarized in Table 1. Permeability ratios were calculated from reversal potentials $V_r$ by use of the equations derived from Goldman–Hodgin–Katz voltage equation:

$$P_{Cl^-}/P_{K^+} = [a_{Kc} - a_{Kt}\exp(-V_r F/RT)]/[a_{Clc}\exp(-V_r F/RT) - a_{Clr}] \quad (8)$$

or

$$P_{Cl^-}/P_{X^+} = a_{Xt}/[a_{Clc}\exp - V_r F/RT)] \quad (9)$$

where $a_{Kc}$ and $a_{Kt}$ are the activities of $K^+$ in the *cis* and the *trans* chambers, $a_{Clc}$ and $a_{Clr}$ the same for $Cl^-$, and $a_{Xt}$ the same for $X^-$.[33]

**Abbreviations and symbols used**: AQ, aqueous; BLM, black (planar) lipid membrane; CD, circular dichroism; $c_F$, free monomer concentration; $c_M$, monomer concentration; CR, central; DOXYL, 4,4-dimethyl-3-oxazolinyloxyl; 5-DOXYL-PC, 1-palmitoyl-2-stearoyl (5-DOXYL)-*sn*-glycero-3-phosphocholine; 12-DOXYL-PC, 1-palmitoyl-2-stearoyl (12-DOXYL)-sn-glycero-3-phosphocholine; EYPC, egg yolk phosphatidylcholine; EYPG, egg yolk phosphatidylglycerol; FDQ, fluorescence depth quenching; $\Gamma$, partition coefficient; HPTS, 8-hydroxypyrene-1,3,6-trisulfonic acid, trisodium salt; IF, interfacial; SUV, small unilamellar vesicle; TM, transmembrane.

## Acknowledgement

We thank the Swiss NSF (21-57059.99 and 2000-064818.01) for financial support.

[1] a) G. Saberwal, R. Nagaraj, *Biochim. Biophys. Acta* **1994**, *1197*, 109–131; b) B. Bechinger, *J. Membr. Biol.* **1997**, *156*, 197–211; c) M. Zasloff, *Nature* **2002**, *415*, 389–395.

[2] a) J. D. Lear, J. P. Schneider, P. K. Kienker, W. F. DeGrado, *J. Am. Chem. Soc.* **1997**, *119*, 3212–3217; b) R. A. Parente, S. Nir, F. C. Szoka Jr., *Biochemistry* **1990**, *29*, 8720–8728; c) G. Menestrina, K.-P. Voges, G. Jung, G. Boheim, *J. Membr. Biol.* **1986**, *93*, 111–132.

[3] a) S. Oiki, R. E. Koeppe II, O. S. Anderson, *Proc. Natl. Acad. Sci. USA* **1995**, *92*, 2121–2125; b) G. A. Woolley, V. Zunic, J. Karanicolas, A. S. Jaikaran, A. V. Starosin, *Biophys. J.* **1997**, *73*, 2465–2475.

[4] N. Sakai, S. Matile, *Chem. Eur. J.* **2000**, *6*, 1731–1737.

[5] a) T. M. Fyles, D. Loock, X. Zhou, *J. Am. Chem. Soc.* **1998**, *120*, 2997–3003; b) C. Goto, M. Yamamura, A. Satake, Y. Kobuke, *J. Am. Chem. Soc.* **2001**, *123*, 12152–12159.

[6] a) J.-Y. Winum, S. Matile, *J. Am. Chem. Soc.* **1999**, *121*, 7961–7962; b) N. Sakai, D. Gerard, S. Matile, *J. Am. Chem. Soc.* **2001**, *123*, 2517–2524.

[7] a) B. Baumeister, N. Sakai, S. Matile, *Angew. Chem.* **2000**, *112*, 2031–2034; *Angew. Chem. Int. Ed.* **2000**, *39*, 1955–1958; b) N. Sakai, B. Baumeister, S. Matile, *ChemBioChem* **2000**, *1*, 123–125.

[8] N. Sakai, S. Matile, *J. Am. Chem. Soc.* **2002**, *124*, 1184–1185.

[9] a) P. Juvvadi, S. Vunnam, R. B. Merrifield, *J. Am. Chem. Soc.* **1996**, *118*, 8989–8997; b) M. Pawlak, S. Stankowski, G. Schwarz, *Biochim. Biophys. Acta* **1991**, *1062*, 94–102; c) S. Stankowski, M. Pawlak, E. Kaisheva, C. H. Robert, G. Schwarz, *Biochim. Biophys. Acta* **1991**, *1069*, 77–86; d) G. Schwarz, G. Beschiaschvili, *Biochim. Biophys. Acta* **1989**, *797*, 82–90; e) W. Hanke, C. Methfessel, H.-U. Wilmsen, E. Katz, G. Jung, G. Boheim, *Biochim. Biophys. Acta* **1983**, *727*, 108–114; f) M. T. Tosteson, D. Tosteson, *Biophys. J.* **1981**, *36*, 109–116.

[10] S. Stankowski, U. D. Schwarz, G. Schwarz, *Biochim. Biophys. Acta* **1988**, *941*, 11–18.

[11] Similar multilabeled vesicle systems have been reported previously: a) K. Venema, R. Gibrat, J.-P. Grouzis, C. Grignon, *Biochim. Biophys. Acta* **1993**, *1146*, 87–96; b) T. Konishi, N. Murakami, Y. Hatano, K. Nakazato, *Biochim. Biophys. Acta* **1986**, *862*, 278–284.

[12] a) A. P. Singh, P. Nicholls, *J. Biochem. Biophys. Meth.* **1985**, *11*, 95–108; b) G. A. Woolley, C. M. Deber, *Biopolymers* **1989**, *28*, 267–272.

[13] P. Linsdell, *J. Physiol.* **2001**, *531*, 51–66.

[14] H. Miedema, *Biophys. J.* **2002**, *82*, 156–159.

[15] a) B. Baumeister, S. Matile, *Chem. Eur. J.* **2000**, *6*, 1739–1749; b) G. Das, S. Matile, *Chirality* **2001**, *13*, 170–176.

[16] In the current context, the term "SUVs" is correct but maybe confusing because the employed vesicles are "very large" SUVs (ca. 68 nm;[17] SUVs: 30–50 nm, LUVs: 100–200 nm; F. M. Menger, K. D. Gabrielson, *Angew. Chem.* **1995**, *107*, 2261–2278; *Angew. Chem. Int. Ed. Engl.* **1995**, *34*, 2091–2106; no significant differences from the activities of **5**/**6** in LUVs prepared by extrusion methods have been observed). The increased curvature of "smaller" SUVs (e.g., 30 nm) influences the function of some membrane-active peptides (see, for example, T. Wieprecht, M. Beyermann, J. Seelig, *Biophys. Chem.* **2002**, *96*, 191–201).

 © 2003 WILEY-VCH Verlag GmbH & Co. KGaA, Weinheim 0947-6539/03/0901-0231 $ 20.00+.50/0 

[17] L. A. Weiss, N. Sakai, B. Ghebremariam, C. Ni, S. Matile, *J. Am. Chem. Soc.* **1997**, *119*, 12142 – 12149.
[18] V. Borisenko, M. S. P. Sansom, G. A. Woolley, *Biophys. J.* **2000**, *78*, 1335 – 1348.
[19] a) G. Das, S. Matile, *Proc. Natl. Acad. Sci. USA* **2002**, *99*, 5183 – 5188; b) G. Das, H. Onouchi, E. Yashima, N. Sakai, S. Matile, *ChemBioChem* **2002**, *3*, 1089 – 1096.
[20] B. Baumeister, N. Sakai, S. Matile, *Org. Lett.* **2001**, *3*, 4229 – 4232.
[21] B. Baumeister, A. Som, G. Das, N. Sakai, F. Vilbois, D. Gerard, S. P. Shahi, S. Matile, *Helv. Chim. Acta* **2002**, *85*, 2740 – 2753.
[22] For comparison of the observed ≈50 ms for the formation of single rigid-rod $\beta$-barrels: the folding of biological $\beta$-barrels in membranes can be very slow if it includes insertion into the bilayer (20 – 30 min; L. K. Tamm, A. Arora, J. H. Kleinschmidt, *J. Biol. Chem.* **2001**, *276*, 32399 – 32402), folding rate constants of water-soluble biological $\beta$-barrels are, depending on barrel size, between 1 ms (T. Schindler, F. X. Schmid, *Biochemistry* **1996**, *35*, 16833 – 16842) to some seconds (C. Roumestand, M. Boyer, L. Guignard, P. Barthe, C. A. Royer, *J. Mol. Biol.* **2001**, *312*, 247 – 259).
[23] L. D. Mayer, M. B. Bally, M. J. Hope, P. R. Cullis, *Biochim. Biophys. Acta* **1985**, *816*, 294 – 302.
[24] P. C. Biggin, J. Breed, H. S. Son, M. S. P. Sansom, *Biophys. J.* **1997**, *72*, 627 – 636.
[25] S. Matile, *Chem. Rec.* **2001**, *1*, 162 – 172.
[26] a) P. S. Phale, A. Philippsen, C. Widmer, V. P. Phale, J. P. Rosenbusch, T. Schirmer, *Biochemistry* **2001**, *40*, 6319 – 6325; b) S. K. Buchanan, *Curr. Opin. Struct. Biol.* **1999**, *9*, 455 – 461; c) C. Lessieur, B. Vécsey-Semjén, L. Abrami, M. Fivaz, F. G. van der Goot, *Mol. Membr. Biol.* **1997**, *14*, 45 – 64.
[27] H. Bayley, P. S. Cremer, *Nature* **2001**, *413*, 226 – 230.
[28] a) K. Matsuzaki, O. Murase, H. Tokuda, N. Fujii, K. Miyajima, *Biochemistry* **1996**, *35*, 11361 – 11368; b) L. Yang, T. A. Harroun, T. M. Weiss, L. Ding, H. W. Huang, *Biophys. J.* **2001**, *81*, 1475 – 1485.
[29] B. Haimovich, J. C. Tanaka, *Biochim. Biophys. Acta* **1995**, *1240*, 149 – 158.
[30] T. Benachir, M. Lafleur, *Biochim. Biophys. Acta* **1995**, *1235*, 452 – 460.
[31] J. Seelig, S. Nebel, P. Ganz, C. Burns, *Biochemistry* **1993**, *32*, 9714 – 9721.
[32] a) D. C. J. Jaikaran, P. C. Biggin, H. Wenschuh, M. S. P. Sansom, G. A. Woolley, *Biochemistry* **1997**, *36*, 13873 – 13881; b) W. Hanke, W.-R. Schlue, *Planar lipid bilayers*, Academic Press, London, **1993**, pp. 111.
[33] a) Z. Qi, M. Sokabe, K. Donowaki, H. Ishida, *Biophys. J.* **1999**, *76*, 631 – 641; b) B. Hille, *Ionic channels of excitable membranes*, 2nd ed., Sinauer, Sunderland, MA (USA), **1992**, pp. 19.

Received: September 6, 2002 [F4402]

 © 2003 WILEY-VCH Verlag GmbH & Co. KGaA, Weinheim 0947-6539/03/0901-0232 $ 20.00+.50/0 